京都大学防災研究所年報 第 67 号 B
DPRI Annuals, No. 67 B, 2024

Comparison of Failure Modes in Benched Slopes Using Centrifugal Models and 3D DEM Simulations

Shanzhi TAO(1), Thirapong PIPATPONGSA(2), Fan ZHU(1) and Yosuke HIGO(1)

(1) Graduate School of Engineering, Kyoto University.
(2) College of Engineering, National Yang Ming Chiao Tung University

Abstract

The stability and failure modes of benched slopes differ from those of slopes with simpler geometry. Centrifugal model tests were conducted to compare the failure modes of benched slopes with varying bench heights under static conditions. To further understand the influencing factors and failure processes in the benched slopes, a three-dimensional discrete element method was used to simulate the centrifuge test. The simulation followed the centrifugal modeling mechanism to reduce computational costs. The results revealed that slopes with a higher first bench were more stable, with failure confined to the bench level. The failure modes of the centrifugal benched slopes were influenced by the water content distribution and the spatial nonuniformity of the centrifugal loading.

Keywords: Benched slope, centrifugal model test, 3D discrete element method

1. Introduction

Slopes with complex geometry commonly exist in roadbed projects (Yang et al., 2021), terraced fields, hilly real estate developments, and open-pit mining (Hustrulid et al., 2001). Tao and Pipatpongsa (2023) investigated the failure mode of laterally confined benched slopes under static loading using centrifugal model tests. They compared the boundary effect by using centrifugal models with distinct breaths. However, the sliding process in the experiment was complex and happened too quickly to be fully captured. Additionally, some details about that experiment need to be supplemented.

To clarify the slope failure mechanism, it is advantageous to utilize the discrete element method (DEM). Jin et al. (2024) highlighted that the DEM facilitates tracking of individual particle movements, providing deeper insights into micro-mechanical behaviors. Wang et al. (2022) emphasized that the DEM offers more detailed particle-scale information, which is often difficult to observe in experiments. However, they also pointed out that this simulation method has a limitation due to its high computational cost, making it challenging to apply in slope failure analysis. To address this issue while retaining the information from the grain size distribution, particles in DEM were often enlarged using the parallel gradation technique (Chang et al., 2013; Salazar et al., 2015). This up-scaling coarse graining approach can be combined with reducing the breath of the model slope and using perfectly smooth side walls (Gabrieli et al., 2009). The periodic boundary can also be used to reduce computation time with decreased dimension of the model (Jin et al., 2024). Those techniques enhance the efficiency of DEM simulations. However, the coarse graining technique dose not adhere to exact scaling laws (Feng and Owen, 2014), and perfectly smooth side walls or periodic boundaries cannot account for the effects of lateral support, which is a crucial factor in centrifugal model tests.

In this study, the centrifugal model test of benched slopes with varying first bench heights was first described. Following this, parameters for the DEM were calibrated using direct shear tests of dry and humid sand. The real grain size distribution curve was applied in the simulation. Two numerical benched slopes were then generated according to the principles of the centrifugal model test, with reduced model dimensions and increased gravitational force. The failure modes of the DEM model slopes were compared with those observed in the experimental test.

2. Centrifugal model test

2.1 Model configuration

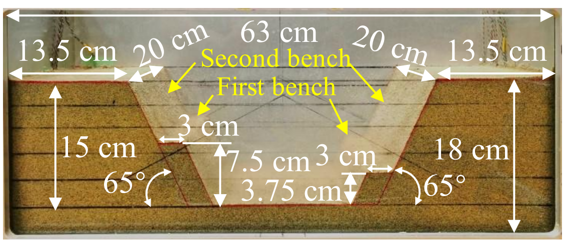

Fig. 1 Physical model used in the centrifuge test (model scale)

To investigate the impact of different first bench heights, two model benched slopes were concurrently tested within a soil chamber. As shown in Fig. 1, the heights of the first benches on the left and right slopes were 7.5 cm and 3.75 cm, respectively, in model scale. The first and second benches on the left slope were equal in height, while the right slope's first bench was half as tall as the left one. Apart from the height of the first bench, all other geometrical parameters of both slopes were identical. The first bench width was 3 cm, the total slope height was 15 cm, the overall model height was 18 cm, the model's breadth was 20 cm, and the distance from the soil chamber wall to the slope crest was 13.5 cm.

2.2 Model preparation

The material used in this study was Hiroshima sand. It is a mountain sand sourced from Kure City, Hiroshima Prefecture, Japan. The raw sand, which initially included gravel, was processed by sieving to remove grains larger than 1 mm to obtain sand suitable for building the model slope. Its classification is between SP (poorly graded sand) and SW (well graded sand) according to the grain size distribution curve (see Fig. 2).

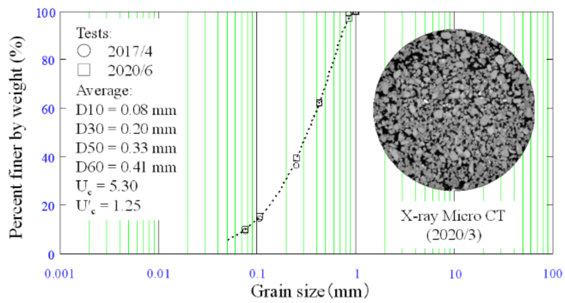

Fig. 2 Grain size distribution of Hiroshima sand after removal of grain size larger than 1 mm

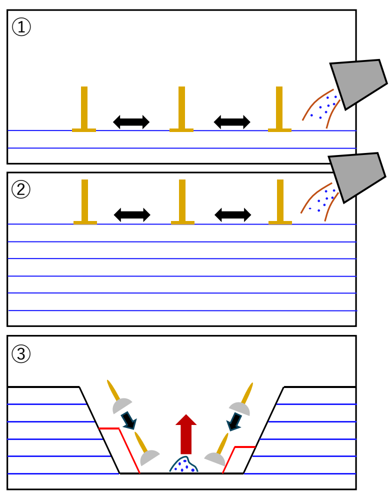

Fig. 3 Process of the model construction

To observe slope failure under static loading conditions with centrifugal acceleration of less than 100G, the slope model was constructed by tamping the Hiroshima sand to an 80% compaction degree (D_c), with a water content (w) of 8%, classifying it as humid sand. The model construction process is illustrated in Fig. 3.

Initially, dry Hiroshima sand was mixed with water to attain the target water content. Subsequently, the sand was divided into six equal portions and compacted into the soil chamber in six layers, each with a thickness of 3 cm, using a wooden hammer. The weight of sand required for each layer was calculated based on the degree of compaction and the volume of the layer. After establishing a horizontal foundation with a height of 18 cm, excessive soil was excavated from the center, and two slope surfaces were shaped using a spatula.

2.3 Test procedure

The constructed model was then installed onto the centrifuge platform for testing. The centrifugal loading was initially increased gradually from 1G to 50G, and thereafter was increased in 10G increments for safety and ease of recording. Once the centrifuge reached the maximum loading of 90G, it was halted, and the centrifugal acceleration was gradually reduced back to 1G. The loading process is depicted in Fig. 4.

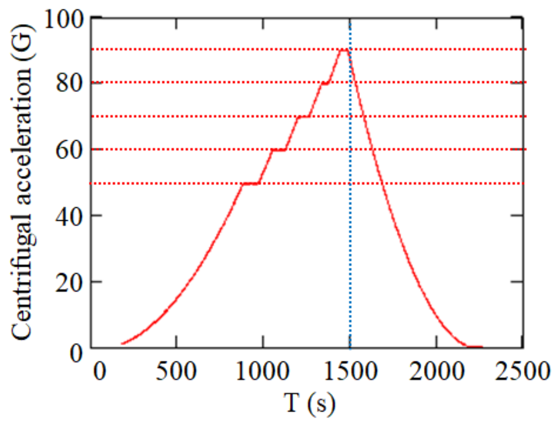

Fig. 4 Centrifugal acceleration with respect to time

2.4 Experimental results

During the test, the slope sliding process was recorded in detail by a high-speed camera. All sliding events occurred within one second are presented in chronological order in Fig. 5.

The first local toe sliding occurred on the right slope at 58G (see Fig. 5 (a)). This was followed by a sliding event at the left first bench near the glass side at 59G (see Fig. 5 (b)) which progressed across the model breadth at 80G (see Fig. 5 (c)). For the right slope, the final local toe sliding happened at 82G, resulting in a complete sliding surface (see Fig. 5 (d)).

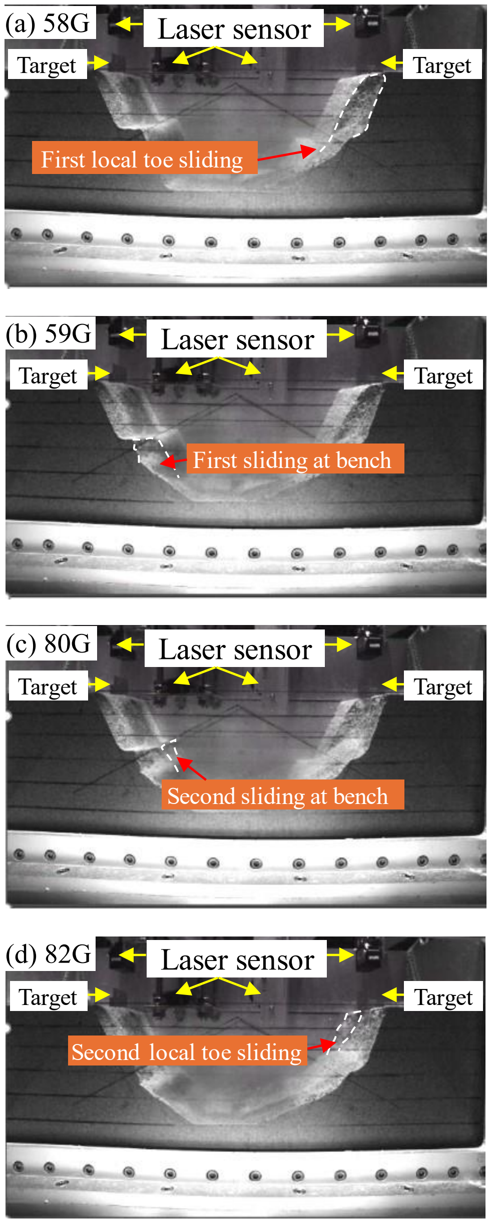

Fig. 5 Process of sliding of benched slopes with increasing centrifugal acceleration

The experimental results indicated that the left slope, with a higher first bench, exhibited greater stability and a different failure mode compared to the right slope, with a lower first bench. Although the initial sliding on the left slope occurred at a similar centrifugal acceleration to that of the right slope (59G compared to 58G), the sliding was confined to the bench level, and the second bench of it remained stable throughout the test. For the right slope, the sliding surface extended from the slope crest down to the slope toe.

Since the main body of the slope behind the first bench was identical for both slopes, the first bench can be considered as a counterweight for the toe. A higher bench with greater weight provided more resisting force to the slope section behind it. Besides, the higher stability of the left second bench, despite having the same height as the first bench, can be attributed to the variation in water content during the test. After the experiment, the water content at different heights of the model slope was measured by taking samples from three distinct levels of the model (see Fig. 6). The water contents at the top, middle, and bottom of the model were 5.5%, 7.3%, and 9.2%, respectively. This distribution of water content resulted from evaporation and gravitational forces during the sample preparation stage, as well as from centrifugal loading during the test. This variation within the model led to differences in shear strength at various slope heights. Another possible reason for this phenomenon is that the centrifugal loading was not uniform across the model height. The upper part of the slope, being closer to the centrifuge pivot, experienced less loading.

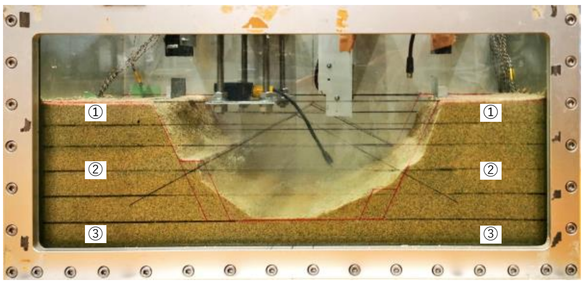

Fig. 6 Water content measurement at different locations after the experiment

3. Numerical simulation based on 3D DEM

To thoroughly elucidate the failure mechanism of benched slopes, the commercial software PFC3D (version 7.00) was used to simulate the centrifugal model as described above.

3.1 Micro parameters calibration

Before simulating the model slopes, the microparameters need to be calibrated. The Adhesive Rolling Resistance Linear Model (ARRLM) (Gilabert et al., 2007; Gilabert et al., 2008) was selected as the contact model between particles to simulate the behavior of sand. A trial-and-error procedure was conducted by adjusting the input microparameters in a series of numerical direct shear tests (NDST) to obtain the parameters that best match the macro-mechanical response observed in experimental direct shear tests (EDST). According to the ARRLM, six microscopic parameters need to be determined. These parameters are effective modulus (E^*), normal-to-shear stiffness ratio (κ^*), friction coefficient (μ), rolling friction coefficient (μ_r), maximum attractive force (F_0), and attraction range (D_0). Not all micro-properties can be calibrated; some must be preselected before the calibration of others. In this study, for all the simulated particles, μ was arbitrarily set to a common value of 0.5, and κ^* was set to 1.5 for simplicity (Sadek et al., 2011; CUI et al., 2022). Therefore, the parameters left to be determined are E^*, μ_r, F_0 and D_0. For the ball-wall contact, a linear model was used with a high E^* of 1 GPa and κ^* of 1.5. The wall in the NDST was assumed to be completely smooth, with μ equal to 0.

In the NDST, a cubic shear box was constructed, comprising twelve PFC3D flat walls (see Fig. 7). Five walls were used to construct the upper part of the shear box, another five walls formed the lower part, and two additional walls were positioned at the shear surface level to prevent particles from escaping during the shear process. For the EDST, the shear box was a cylinder, with a diameter of 0.06 m and a height of 0.02 m. These dimensions were converted to the width and height of the cubic box by multiplying a coefficient of 0.22 as shown in Fig. 7(a). This coefficient was chosen to reduce the box size, thereby keeping the number of particles within a reasonable range, given the constraints of computational capacity.

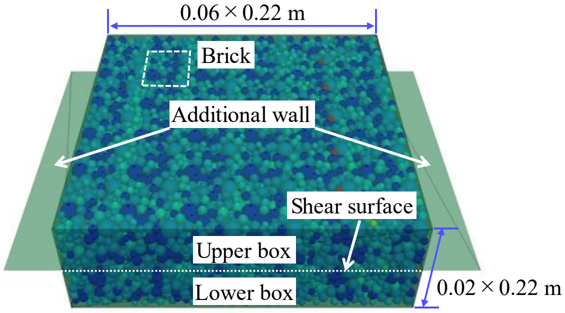

(a) Before shearing

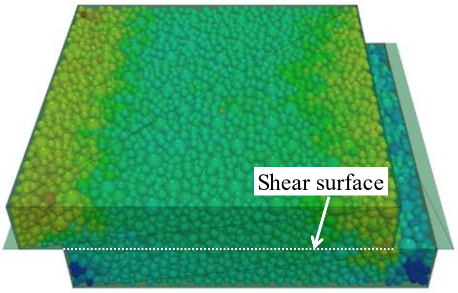

(b) After shearing

Fig. 7 Shear box with model particles in NDST

PFC3D can create a particle assembly based on the designated grain size distribution curve and porosity using the 'ball distribute' command. To enhance the homogeneity of the specimen, a brick, which is an assembly of particles arranged within a periodic space, was created first. Then, this brick was replicated multiple times to construct the specimen (see Fig. 7 (a)).

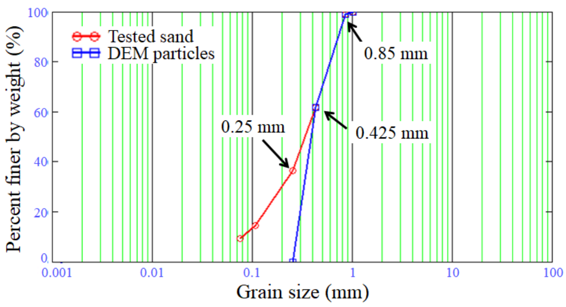

Fig. 8 Comparison of grain size distribution curves between real sand and DEM particles

Fig. 8 shows a comparison of the grain size distribution between the real sand and the DEM model. Particles with diameters less than 0.25 mm were excluded from the simulation, and their volume percentage was incorporated into the 0.25 mm to 0.425 mm range to reduce computational costs. The median particle diameter d_{50} in the simulation was 0.39 mm, which is slightly larger than the D_{50} of 0.33 mm for the real sand (see Fig. 2). The ratio of the numerical shear box height, which was the smallest characteristic model length, to the median diameter of the DEM particle (L/d_{50}) was 11. This value was sufficiently large to avoid the boundary effect (Zhang et al., 2018). The shear displacement rate for the EDST was 0.2 mm/min, which was increased by a factor of 1000 for the NDST. The selected loading rate did not bring apparent inertia effect in the simulation.

Initially, the simulation was conducted for the dry Hiroshima sand with a compaction degree of 80%. The DEM particles were assigned the same particle density as the real Hiroshima sand (2633 kg/m^3). The porosity of the sample was calculated using the particle density and the bulk density. A total of 13,284 particles were generated for the specimen. At first, μ_r, F_0 and D_0 were set to zero, and E^* was set to a common value of 100 MPa. The values of μ_r and E^* were adjusted iteratively to align the virtual stress-strain curves with the real ones. Ultimately, μ_r=0.16 and E^*=300 MPa were determined. During the consolidation stage of the NDST, the upper box was fixed, and normal pressure was applied to the bottom wall of the lower box, consistent with the procedure used in the EDST. During shearing, this pressure was maintained constant using a servo command, and the upper box moved to the left to shear the specimen.

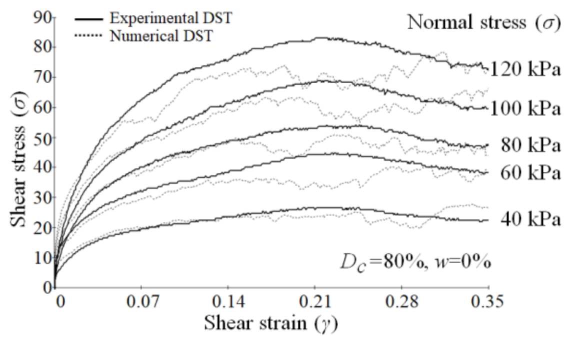

Fig. 9 Shear stress – shear strain curves under different normal pressures for the dry sand

Fig. 9 shows the stress-strain curves from both EDST and NDST for dry sand samples, after calibration, under different confining pressures of

40, 60, 80, 100, and 120 kPa.

Due to matric suction, the humid Hiroshima sand used for the model slope exhibits higher strength compared to the dry sand. Here, the F_0 and D_0 were calibrated to account for the additional cohesion resulting from the suction. Those two parameters were set to non-zero values only for contacts established before shearing; any newly created contacts during shearing were assigned a value of zero. Since the water content decreased in most parts of the slope, EDST with D_c=80% and w=6% were used for calibrating the humid sand. The results are F_0=1.2×10^{-4} N and D_0=0.

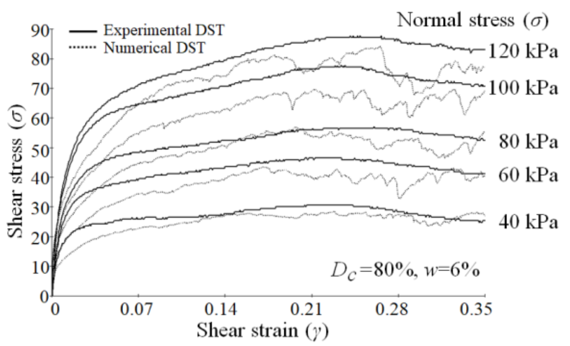

Fig. 10 Shear stress – shear strain curves under different normal pressures for the humid sand

Table 1 Material properties of DEM analysis

	Material property	Value (units)
Ball	Density	2633 kg/m^3
	Damping ratio	0.7
Ball-ball	Effective modulus (E^*)	300 MPa
	Normal-to-shear stiffness ratio (κ^*)	1.5
	Friction coefficient (μ)	0.5
	rolling friction coefficient (μ_r)	0.16
	Maximum attractive force (F_0)	1.2×10^{-4} N
	Attraction range (D_0)	0 m
Ball-wall	Effective modulus (E^*)	1 GPa
	Normal-to-shear stiffness ratio (κ^*)	1.5
	Friction coefficient (μ)	0

Fig. 10 shows the stress-strain curves from both EDST and NDST for humid sand samples after calibration. Finally, the material properties obtained from the calibration are summarized in Table 1.

3.2 Setup of the DEM benched slope model

Following the sample generation method used in the NDST, a cubic sample was generated to represent the foundation of the centrifugal model, as depicted in step 1 in Fig. 3. Its dimensions were determined by taking half the length of the actual foundation, as it was intended to simulate only one model slope. Then, all dimensions were multiplied by a size reduction factor of 0.063 to reduce the total number of particles. The total number of generated particles is 47,070.

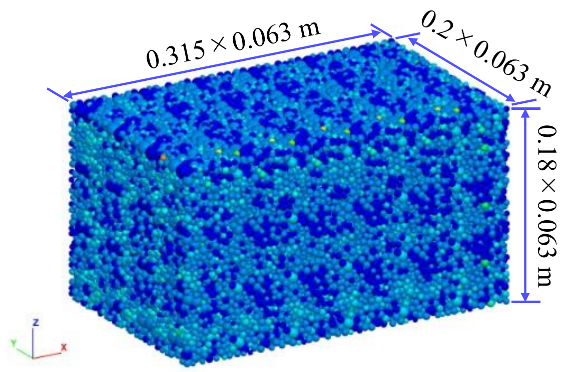

Fig. 11 Dimensions of the foundation in DEM

For the foundation sample, L/d_{50}=32. While most parameters in the simulation of the benched slopes remained consistent with those used in the NDST, the ball-wall friction (μ) was set to 0.2 to account for the lateral resistance provided by the wall of the soil chamber. Additionally, F_0 was divided by the size reduction factor (0.063) to compensate the loss of cohesion due to the reduced dimensions of the numerical model compared to the centrifugal model.

In the centrifugal model test, the foundation was initially cut to shape the slope surface, after which the model slope was subjected to increasing centrifugal loading. The entire loading process took approximately 1500 s (see Fig. 4). Simulating the exact loading process can be time consuming and impractical in DEM. To address this issue, the foundation in the simulation was first loaded by an increased gravitational force to reach an equilibrium state. Then, part of the particles was removed to form the benched slope. Subsequently, the benched slope is loaded to deform under the increased gravitational force, which mimics the centrifugal loading in the model test. In the centrifugal model, the centrifugal loading is equivalent to the gravitational force multiplied by a scaling factor (n). In the simulation, this scaling factor was further increased by dividing it with the size reduction factor (0.063) to achieve a stress state similar to that of the centrifugal model (i.e., the simulated slope and the centrifugal model slope have the same prototype size).

3.3 Simulation results

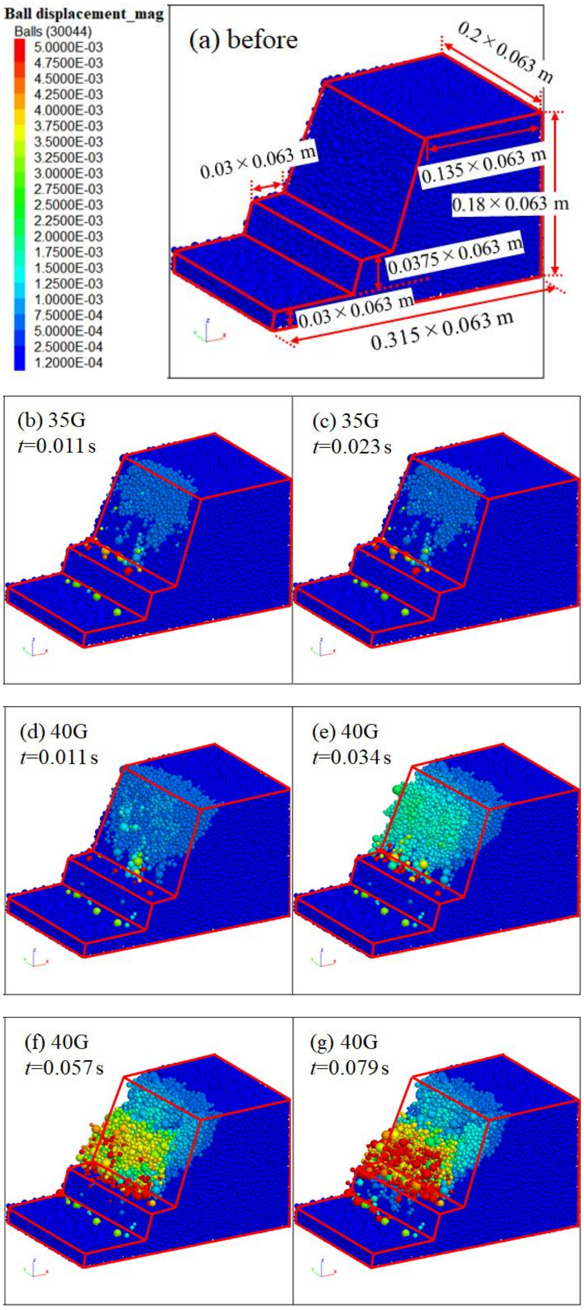

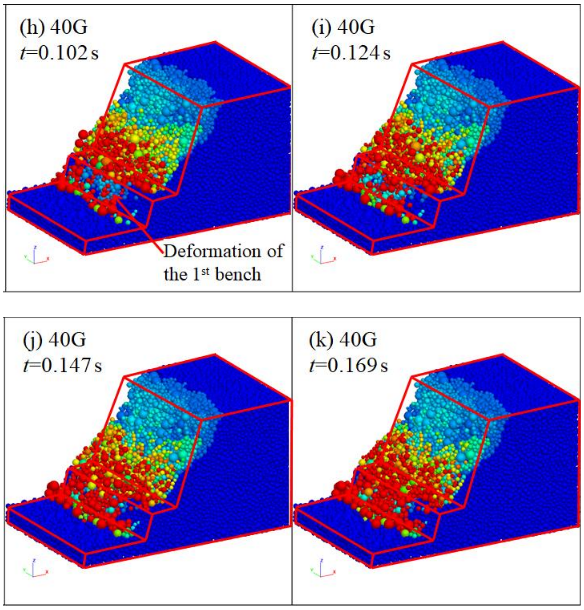

Fig. 12 Sliding process of benched slopes with the lower bench simulated by DEM

The benched slope with the lower bench on the right-hand side of the centrifugal model was simulated first, as shown in Fig. 12. The Fig. 12 (a) illustrates the state of the slope immediately after removing the undesirable particles (i.e., at the formation of the benched slope). The benched slope was modeled with 30,044 particles in total. The accumulated displacement during both the specimen generation and loading processes was reset to zero to facilitate the observation of the subsequent sliding process. The maximum and minimum values of the displacement were set to 5×10^{-3} m and 1.2×10^{-4} m, respectively, which cover the displacement range of most particles. The outline of the undeformed slope was indicated by red lines. The centrifugal loading shown in each subgraph is the equivalent value used in the centrifugal model test. Yang et al. (2014), and Chiu and Weng (2019) noted that the friction coefficient between the sliding block and the sliding surface decreased as the velocity increased. Therefore, μ_r was set to zero for all new ball-ball contact established during the sliding process.

When a loading of 35G was applied to the model, deformation began at the slope crest (see Fig. 12 (b)). Although a few particles rolled down, no distinct sliding surface was formed, and the slope stabilized after 0.023 s (see Fig. 12 (c)). Next, the loading on the foundation was increased to 40G, and the sliding process was simulated once more. The displacement figure was selected with an interval of 1×10^5 timesteps. After part of particles were removed to shape the slope surface, deformation began at the slope crest (see Fig. 12 (d)), followed by sliding in the front part of the deformed area (see Fig. 12 (e)). This sliding was confined to the second bench of the slope until part of the first bench was destroyed by the sliding body in 0.102 s (see Fig. 12 (h)). Eventually, the sliding body covered the first bench, and the model nearly reached equilibrium (see Fig. 12 (k)). The state of the slope remained largely unchanged afterward, so the subsequent graphs are not presented.

The simulated centrifugal loading required to fail the simulated slope was 40G, which deviates from the 58G observed in the centrifugal model. It may be caused by reduced centrifugal loading of the second bench in the centrifugal model. Additionally, in the simulation, the sliding surface extended across the entire model breadth, whereas only a portion of the slope failed during the first sliding in the centrifugal model. This difference is attributed to the fact that the centrifugal model was compacted by hand, leading to inevitable inhomogeneity. The area of the model near the wall was less compacted than the central part.

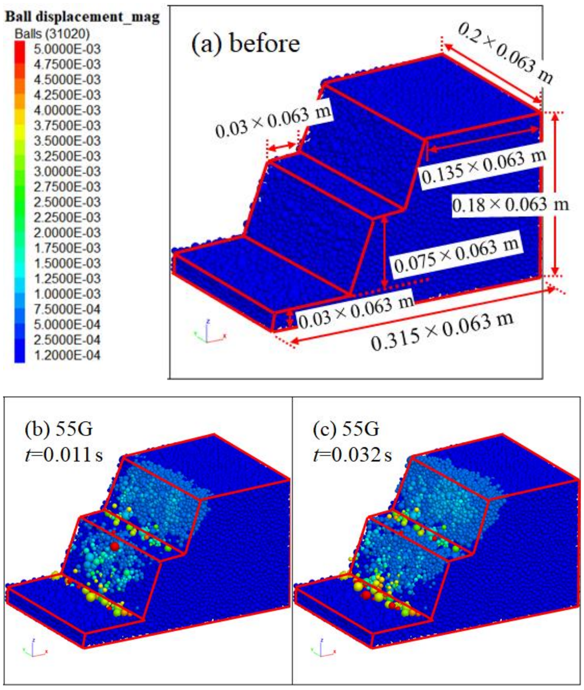

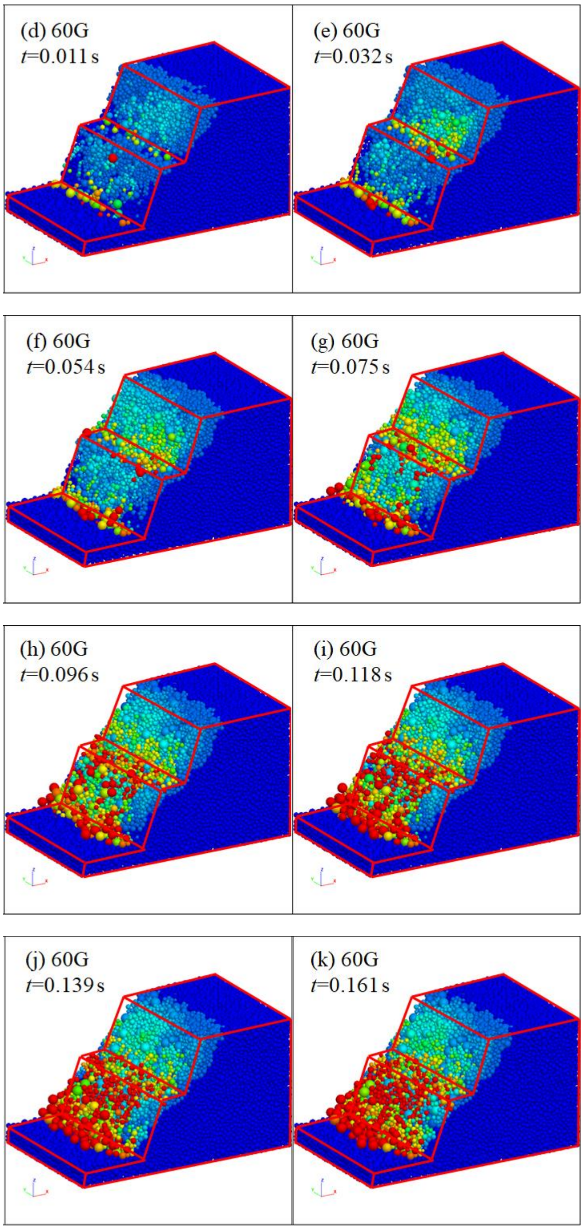

Fig. 13 Sliding process of benched slopes with the higher bench simulated by DEM

The benched slope with the higher bench on the left-hand side of the centrifugal model was then simulated, as shown in Fig. 13. Fig. 13 (a) illustrates the state of slope immediately after the formation of the benched slope. Similar to the simulation of the benched slope with a lower bench, the accumulated displacement was reinitialized, and the same displacement range was adopted. A total of 31,020 particles were simulated for the benched slope.

When a loading of 55G was applied to the model, deformation began simultaneously in the front areas of the first and second benches (see Fig.

13 (b)). Within 0.032 s, the slope stabilized with increased deformation and some particles rolled down (see Fig. 13 (c)). Subsequently, the loading was increased to 60G. The slope exhibited more deformation in Fig. 13 (d) compared to Fig. 13 (b), even though the same duration of 0.011 s was taken. Deformation continued to develop until 0.075 s, at which point sliding began simultaneously on the first and second benches. Finally, the sliding body accumulated at the toe of the slope, and the model approached a near equilibrium state (see Fig. 13 (k)). The state of the slope remained largely unchanged afterward, so the subsequent graphs are not included.

The simulated centrifugal loading required to fail the slope was 60G, which is nearly the same as the 59G observed in the centrifugal model. However, the failure mode observed in the simulation differed from that in the centrifugal model test. In the simulation, both the first and second benches failed simultaneously, whereas the second bench remained stable in the centrifugal test. The slope in the DEM simulation was more homogeneous compared to the real slope. Additionally, the simulated centrifugal loading was uniform across all particles, whereas in the centrifugal test, the loading varied with height.

4. Conclusions

This study investigated the failure modes of benched slopes with varying first bench heights by comparing the results of centrifugal model tests and 3D DEM simulation. DEM can effectively simulate large deformation processes and accurately capture the details of slope sliding. The parameters of the DEM model were calibrated using direct shear tests to determine the contact properties. Simulations of both dry sand and humid sand showed good agreement with the experimental data. During the benched slope simulation, the entire slope sliding process was captured, including the initiation area, sliding surface, and final state. The major conclusions drawn from this study are summarized as follows:

(1) With all other geometric parameters being identical, the benched slope with a higher first bench was more stable due to the increased resisting force provided by the larger toe counterweight.

(2) For the benched slope with a high bench, failure was confined to the bench level. In contrast, the failure surface of the benched slope with a low bench extended from the slope crest to the slope toe.

(3) The failure mode of centrifugal model slopes was affected by the distribution of water content, as well as the variation of the centrifugal loading with the height. It was demonstrated by the DEM simulation.

(4) DEM simulations can achieve good consistency with centrifugal model tests by reducing the model size and increasing the gravitational force. This approach maintains a similar stress state in the simulation to that of the real model, while allowing the use of particles comparable in size to the real sand and controlling the number of particles in the simulation to reduce computational cost.

Acknowledgements

This research was gratefully supported by JSPS KAKENHI Grant Number 20H02242. Thanks are extended to Mr. A Siga and Mr. Pongsakorn Wongchana for their assistance with the experiments.

References

Chang, Y. Y., Lee, C. J., Huang, W. C., Huang, W. J., Lin, M. L., Hung, W. Y., and Lin, Y. H. (2013): Use of centrifuge experiments and discrete element analysis to model the reverse fault slip, International Journal of Civil Engineering, Vol. 11, No. 2, pp. 79-89.

Chiu, C.-C., and Weng, M.-C. (2019): DEM simulation of planar sliding using a particulate interface model considering velocity-dependent friction, Computers and Geotechnics, Vol. 112, pp. 51-59.

CUI, P.B., ZHU, Y.Q., LIU, Y., ZHU, Z.G. and PAN, Y.D. (2022): Model test and particle flow numerical simulation of soil arching effect for unsaturated sandy soil tunnel, Rock and Soil Mechanics, Vol. 42, No. 12, p. 7.

Feng, Y. T., and Owen, D. R. J. (2014): Discrete element modelling of large scale particle systems—I: exact scaling laws, Computational Particle Mechanics, Vol. 1, No. 2, pp. 159-168.
Gabrieli, F., Cola, S., and Calvetti, F. (2009): Use of an up-scaled DEM model for analysing the behaviour of a shallow foundation on a model slope, Geomechanics and Geoengineering, Vol. 4, No. 2, pp. 109-122.
Gilabert, F.A., Roux, J.-N. and Castellanos, A. (2007): Computer Simulation of Model Cohesive Powders: Influence of Assembling Procedure and Contact Laws on Low Consolidation States, Physical Review E, Vol. 75.
Gilabert, F.A., Roux,J.-N. and Castellanos, A. (2008): Computer Simulation of Model Cohesive Powders: Plastic Consolidation, Structural Changes and Elasticity under Isotropic Loads, Physical Review E, Vol. 78.
Hustrulid, W. A., McCarter, M. K., and Zyl, D. J. A. V. (2001): Slope stability in surface mining. Englewood.
Jin, X., Li, X., and Huang, Y. (2024): DEM analysis on diffuse failure of soil slope triggered by earthquakes, Engineering Geology, Vol. 339.
Sadek, M.A., Chen, Y. and Liu, J. (2011): Simulating shear behavior of a sandy soil under different soil conditions, Journal of Terramechanics, Vol. 48, No. 6, pp. 451-458
Salazar, A., Sáez, E., and Pardo, G. (2015): Modeling the direct shear test of a coarse sand using the 3D Discrete Element Method with a rolling friction model, Computers and Geotechnics, Vol. 67, pp. 83-93.
Tao, S., and Pipatpongsa, T. (2023): Characteristics of reduction factors for lateral confining pressure of a benched slope in centrifuge model tests, Proceedings of the Conference on Computational Engineering and Science.
Wang, D., Wang, B., Jiang, Q., Guo, N., Zhang, W., and He, K. (2022): Large deformation slope failure — A perspective from multiscale modelling, Computers and Geotechnics, Vol. 150.
Yang, C.-M., Yu, W.-L., Dong, J.-J., Kuo, C.-Y., Shimamoto, T., Lee, C.-T., Togo, T., and Miyamoto, Y. (2014): Initiation, movement, and run-out of the giant Tsaoling landslide — What can we learn from a simple rigid block model and a velocity–displacement dependent friction law? Engineering Geology, Vol. 182, pp.158-181.
Yang, S., Wang, Z., Wang, J., Gong, M., Li, J., and Sun, Z. (2021): 3D seismic stability analysis of bench slope with pile reinforcement, Geotechnical and Geological Engineering, Vol. 40, No. 3, pp. 1149-1163.
Zhang, Z., Cui, Y., Chan, D. H., and Taslagyan, K. A. (2018): DEM simulation of shear vibrational fluidization of granular material, Granular Matter, Vol. 20, No. 4.

(Received August 31, 2024)